

Electrodeposition of Fe–Co alloys into nanoporous *p*-type silicon: Influence of the electrolyte composition

F. Hamadache^{a)}

Unité de Physico-Chimie et de Physique des Matériaux, Université Catholique de Louvain, Croix du Sud 1, B-1348 Louvain-la-Neuve, Belgique

J-L. Duvaill

Laboratoire de Physique Cristalline, Institut des Matériaux de Nantes, 2, Rue de la Houssinière, 44322 Nantes cedex 03, France

V. Scheuren

Laboratoire de Microélectronique, Université Catholique de Louvain, Place du Levant 3, B-1348 Louvain-la-Neuve, Belgique

L. Piraux, C. Poleunis, and P. Bertrand

Unité de Physico-Chimie et de Physique des Matériaux, Université Catholique de Louvain, Croix du Sud 1, B-1348 Louvain-la-Neuve, Belgique

M.S. Belkaïd

Laboratoire de Microélectronique Appliquée, Université Mouloud Mammeri de Tizi-Ouzou, Campus Universitaire Hasnaoua, 15000 Tizi-Ouzou, Algérie

(Received 5 April 2001; accepted 14 February 2002)

The cathodic deposition of iron–cobalt alloys inside the pores of anodically formed nanoporous silicon (PS) from *p*-type Si substrate is investigated with respect to the electrolyte composition. The samples were characterized by scanning electron microscopy, energy dispersive spectrometry, Auger electron spectroscopy, and Fourier transform infrared spectroscopy. Results showed that the nucleation of pure cobalt started at the bottom of the pores and the nucleation of pure iron occurred all over the pore walls, leading to a preferential deposition on top surface of the porous layer. Nevertheless, a low concentration of Co²⁺ ions (5 at.%) in the electrolyte drastically improved the penetration of iron into the pores. As a result, a good filling of the pores with Co metal as well as with Fe–Co alloys was achieved. It was also shown that the deposition process oxidizes the structure mainly at the pore walls. The results of our investigation indicate that the mechanisms occurring during the electrodeposition of metals on porous *p*-type silicon substrates are completely different depending on the kind of electrolyte used: pure iron-based electrolyte or cobalt-based solutions. A complete understanding of the deposition process requires further analyses of the carrier transport in PS and of the charge exchange at the Si/electrolyte and PS/electrolyte interfaces. These new results involving the deposition of iron-group materials into porous *p*-type silicon are useful for future silicon technologies.

I. INTRODUCTION

Recently, much effort has been devoted to the impregnation of porous silicon (PS) with different materials.¹ Dealing with the introduction of metals into the pores,^{2–14} special attention was paid to the realization of deep electrical contact with the pore walls to improve the electroluminescence efficiency.^{4–6,8} The substitution of easily

broken Si–H bonds with solid metal–Si ones has also been of concern to stabilize the luminescence properties of this material.^{3–7} Nevertheless, another remarkable property of PS that may open more future prospects to silicon technology lies in that one can get a PS structure with cylindrical pores parallel each other and perpendicular to the surface. Indeed, the introduction of ferromagnetic iron-group metals in a such PS structure would lead to new potential systems for magnetic memory, storage disk, and microwave applications.^{2,10} For the commonly used templates, i.e. track-etched polymer membranes and porous alumina, the fabrication and

^{a)}Present address: Département des Matériaux et Composants, Université des Sciences et de la Technologie Houari Boumédiène, B.P. 32 El-Alia, 16111 Bab-Ezzouar Alger, Algérie.

properties of arrays of magnetic nanowires and multilayers have aroused a considerable interest during the last decade.^{15–17} When compared to the other nanoporous materials, the pertinent advantages of PS are its very low cost and compatible post-integration in a CMOS process, which is a major requirement for commercial devices.² Furthermore, the achievement of a suitable metallization of PS with iron or other metals to fabricate buried conductive and semiconductive silicide layers inside single-crystal silicon always remains an open topic.^{3,4,9,11–14}

The filling of porous silicon with different materials is not an easy task. Electrochemical deposition constitutes an attractive method to fill the pores in a controlled way.^{1,4,6,8} However, scattered results were obtained regarding the in-depth profile concentration of the electrodeposited metals. These differences can be assigned either to changes in the pore shape or to a hydrogen evolution side reaction, which both may lead to pore blockage. It is believed, however, that the nature of the metal and the type of silicon doping seem to be the more determinant parameters. Indium has been successfully introduced in the volume of the porous *n*-type silicon,⁸ while it has been deposited on top surface when porous *p*-type silicon is used.⁷ A reverse situation has been reported in the case of ZnSe.¹

Iron deposition into PS layer formed on *n*-type Si has been initiated by Ronkel and co-workers.⁴ Despite their use of porous silicon with a spongelike shape and the high rate of hydrogen evolution observed, a relatively homogeneous pore filling has been achieved. More recently, Renaux and co-workers have reported on electrodeposition of iron into PS prepared with *p*-type Si wafers (*p*-Si is preferentially used as substrate than *n*-Si in microelectronic devices).² They concluded that iron nucleation occurs all over the pore walls, resulting in a quick pinching of the pores.

Cobalt is another iron-group metal that was also deposited into porous silicon but by using the CVD technique.^{5,11} As this metal is more noble than iron, it is expected that it will catalyze iron inside the pores of porous *p*-type Si making up Fe–Co compounds.¹⁸ These alloys have also a wide range of applications in magnetic data recording storage and printing devices.^{18–21} In other respects, the interest for one of the more important silicides for silicon technology, β -FeSi₂, is now shifted toward the ternary phases Fe_{1-x}Co_xSi₂ that have better semiconductor properties.^{22–24}

This work reports on the impregnation of cylindrical-like shape nanoporous *p*-type Si by electrodeposited Fe–Co alloys, in comparison with their related pure metals. It shows, in particular, that an incorporation of just a small amount of cobalt sulfate in iron sulfate-based electrolyte can successfully improve the penetration of iron into the pores. The structure of the porous silicon layer and its impregnation with the electrodeposit were

examined by scanning electron microscopy (SEM). The average composition of the deposit was determined by energy dispersive spectrometry (EDS). The distribution of the different elements in the porous layer was studied by Auger electron spectroscopy (AES). Some chemical bonds present in the samples were identified by Fourier transform infrared spectroscopy (FTIR).

II. EXPERIMENTAL PROCEDURES

A. Sample preparation

Our experiments were carried out through an O-ring-sealed window (about 0.5 cm² area) of an electrochemical single cell. The back side of the substrate was pressed against a silver electrode for electrical contact, whereas its front side was exposed to the electrolyte. A pure Pt counter-electrode was immersed in the electrolyte to supply electrical current toward the sample by means of a programmable Keithley model 224 current source.

The starting (100)-oriented silicon wafers are B-doped (*p*-type) with a resistivity of 15–25 Ω cm. Prior to the PS formation, a heavily B-doped (*p*⁺) layer of typically 10¹⁹ cm⁻³ in carrier concentration and 0.5 μ m in depth was formed on both sides of the wafers. Such a doping is necessary, both to ensure good ohmic contact and to produce cylindrical nanoscale pores at the front side, which is a requirement for a complete filling of the pores.¹ The *p*⁺ layer has been obtained by implantation of the wafers with 110-keV B⁺ ions at a dose of 1 \times 10¹⁶ at/cm³ followed by an annealing at 950 °C during 30 min. After implantation, the wafers were cleaned following the IC standard procedure and cleaved to 1.2 \times 1.2 cm² samples.

The samples were first cleaned with 2-propanol, immersed in 5% HF for a few seconds, rinsed with deionized water, and dried by N₂ to remove the native oxide layer. They were then etched under galvanostatic conditions in an electrolyte composed of 30 vol% hydrofluoric acid (49 wt%) and 70 vol% ethanol (i.e., in 15% HF–EtOH electrolyte) to form the porous layer. Two different porosities of approximately 80% and 60% have been obtained by applying a current density of 3 and 0.3 mA/cm², respectively. After the formation, PS samples were wetted with ethanol and etched in 5% HF for a few seconds to remove any oxide layer. Then they were rinsed with deionized water and immersed again in ethanol to facilitate removal of any excess electrolyte by evacuation to 10⁻²–10⁻³ torr for 1 h. After that, the porous silicon is exposed to the deposition bath for 10 min to ensure good pore penetration by the aqueous electrolyte.

The filling of the porous silicon layer by iron and cobalt was also performed at a constant current mode. The polarity of the power source was then reversed, and a current density of 500 μ A/cm⁻² was supplied. Iron

and cobalt were codeposited from an aqueous solution prepared by dissolving iron sulfate ($\text{FeSO}_4 \cdot 7\text{H}_2\text{O}$) and cobalt sulfate ($\text{CoSO}_4 \cdot 7\text{H}_2\text{O}$) in deionized water containing boric acid with a concentration of 0.4 M. The sum of Fe^{2+} and Co^{2+} ions concentration in this solution was kept equal to 0.1 M, while the relative concentration of both ions was changed in the range of 0–0.1 M. The pH is always kept close to 3 by adding sulfuric acid in order to avoid the formation of the hydroxides.

Both anodization of silicon and Fe–Co electrodeposition were performed at room temperature and without agitation. They were also carried out in the dark to avoid the oxidation of PS via the known reaction by injection current multiplication.^{6,8}

B. Sample characterization

The pores size and the thickness of the porous layer, as well as the presence of the deposit in the pores, were determined from the sample cross-section images obtained by a DSM982 GEMINI scanning electron microscope (SEM). The energy-dispersive spectroscopy (EDS) analysis performed at 15 kV was used to determine the average composition of the deposits. However, only qualitative study of the pores filling can be made with SEM. EDS is no longer a suitable technique to determine the in-depth distribution of the metals because of its relatively low spatial resolution. Therefore, in the case of our 0.3- μm -thick samples, the metal concentration profiles in the porous layer were analyzed by Auger electron spectroscopy (AES) in a PHI model 600 Multiprobe from Perkin-Elmer. The Auger spectra were recorded with a primary electron beam of 3 keV and 0.4 μA incident at 45° angle. Depth profiling was carried out using 2-keV Ar^+ sputtering with a current density of 250 $\mu\text{A cm}^{-2}$. The Fe, Co, Si, O, and C concentrations were measured using the peak-to-peak-height (APPH) analysis of the Auger Fe LMM (600 eV), Co LMM (777 eV), Si LVV (96 eV), O KLL (510 eV), and C KLL (275 eV) electron peaks, respectively. The corresponding relative sensitivity factors used are respectively 0.144, 0.300, 0.414, 0.338, and 0.165 at 3 keV.²⁵ The chemical composition of the internal surface of the as-formed and metallized porous silicon was examined using Fourier transform IR spectroscopy (FTIR) with a resolution of 4 cm^{-1} . The FTIR analyses were achieved in air just after the sample preparation.

III. RESULTS

A. Cyclic voltammetry study

Preliminary experiments were made to determine the deposition potential of iron and cobalt. They consist in sweeping the potential of the substrate (scan rate: 20 mV s^{-1}) in contact with solutions containing different

amounts of the Fe^{2+} and Co^{2+} species. These experiments were carried out with an EGG 270/250 potentiostat/galvanostat, and the potential was measured against a standard Ag–AgCl reference electrode. The results (curves are not reported here) show that the current density presents a single peak at a cathodic potential around -0.85 V/Ag–AgCl , whatever the Fe^{2+} concentration ranging between 0 and 1 M.

B. Electron scanning microscopy (SEM)

The starting substrate used for iron and cobalt deposition is a freshly prepared porous silicon. Figure 1 shows a cross-section SEM image of (a) an as-prepared PS and (b) a PS impregnated with Fe–Co alloy. In both cases, the porous silicon was prepared by anodizing a p^+ -type and (100)-oriented Si substrate in a 15% HF–EtOH electrolyte at a current density of 0.3 mA cm^{-2} . Under these conditions, the PS layer thickness increases at a rate of 15 nm min^{-1} and its structure presents a high pore density [$(5\text{--}7) \times 10^2 \mu\text{m}^{-2}$]. As a result, a layer of 60% porosity is obtained. The pores are uniform in length and formed straight perpendicularly to the surface. They have however ink-bottle shapes, resulting from the heterogeneity of the implantation near the surface. To achieve a cylindrical pore structure and then to facilitate the penetration of the deposit into the porous layer, the

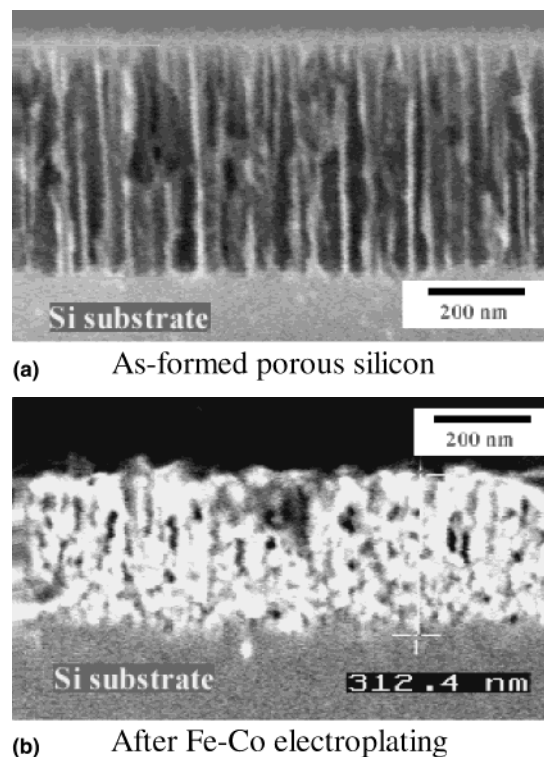


FIG. 1. Cross-section SEM image of porous *p*-type silicon (60% porosity): electrolytes, HF–ethanol (3:7); etching current density, 0.3 mA cm^{-2} for PS preparation; 0.075 M Fe^{2+} and 0.025 M Co^{2+} ; cathodic current density, 500 $\mu\text{A cm}^{-2}$ for Fe–Co electrodeposition.

pores are easily widened at the surface by a method described in Ref. 2. Porous layers of approximately 0.3- μm thickness were electroplated with Fe–Co deposit [Fig. 1(b)]. The deposit is obtained from an iron-rich solution composed of 0.075 M Fe^{2+} plus 0.025 M Co^{2+} under cathodic polarization at a current density of 500 $\mu\text{A}/\text{cm}^2$ during 10 min. After the electrodeposition,

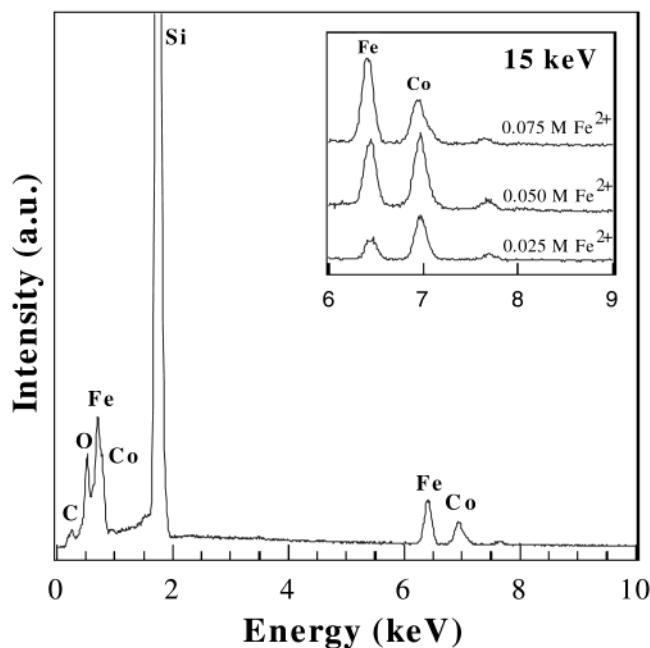


FIG. 2. X-ray energy-dispersive spectrometry analysis of a 0.3- μm porous (60%) *p*-type silicon layer after Fe–Co deposition from electrolytes with different Fe^{2+} and Co^{2+} concentrations.

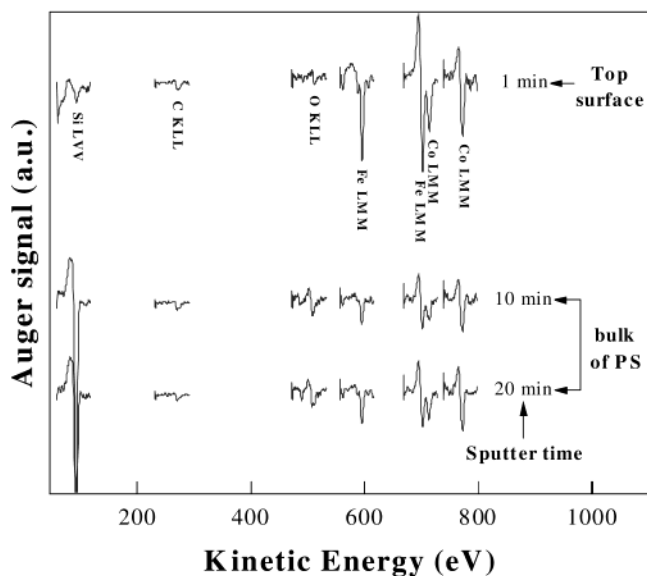


FIG. 3. AES signatures at three different sputter times of silicon, iron, cobalt, oxygen, and carbon in a 0.3- μm porous (60%) *p*-type silicon layer after Fe–Co deposition from a 0.075 M Fe^{2+} and 0.025 M Co^{2+} electrolyte.

the PS layer becomes brighter all along its thickness. This is a strong indication that the entire layer is impregnated with the deposit, which will be confirmed in the following by AES analysis (Sec. III.D).

C. Energy dispersive spectrometry (EDS)

The presence of both Fe and Co metals in the deposit is revealed by energy dispersive spectrometry (EDS) analysis. A typical EDS spectrum recorded between 0 and 10 keV (Fig. 2) indicates that the samples contain, in addition to silicon, iron, cobalt, oxygen, and a bit of carbon. From the inset, it has been possible to estimate quantitatively the average compositions of the deposits obtained for three compositions of the electrolyte. The iron composition in the deposits, defined as the ratio between iron and the total (Fe + Co) content, is about 24, 44, and 61 at.% Fe for the electrolyte composition of 25, 50, and 75 mol% Fe^{2+3} , respectively. From these values, it appears that iron-poor deposits with respect to the bath composition are formed. Curiously, the deficit of iron in the Fe–Co deposit is increasing with the ferrous ion concentration of the solution. This point will be discussed later, in view of additional results.

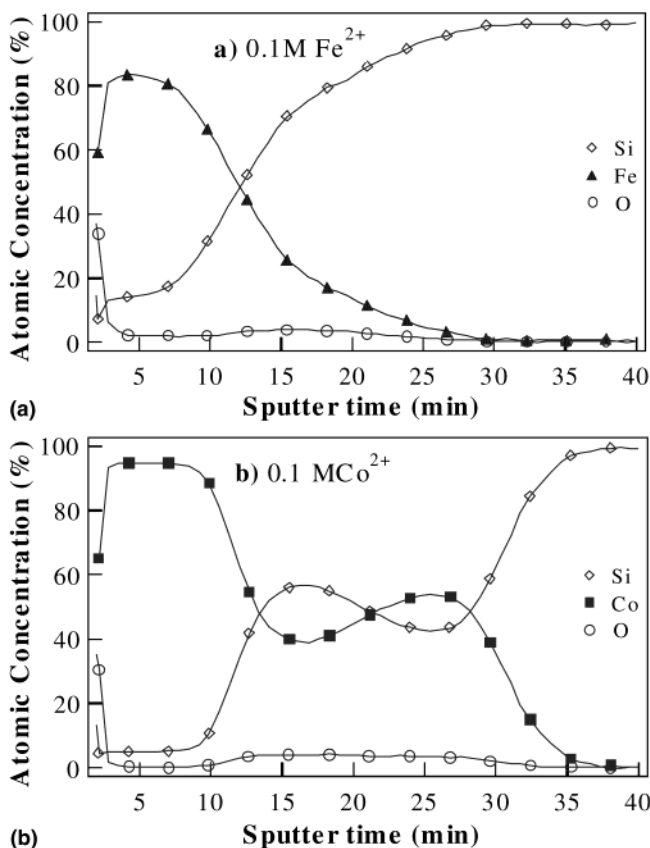


FIG. 4. Auger depth profiles of iron, cobalt, silicon, and oxygen performed by ion etching in a 0.3- μm *p*-type porous layer electroplated by (a) pure iron or (b) pure cobalt.

D. Auger electron spectroscopy (AES)

The depth distribution of Fe and Co metals deposited into PS was measured by the AES technique. Figure 3 shows the signature of the different elements present on top surface layer (after 1 min in etching by ionic abrasion) and in the bulk of PS (after 10 and 20 min in etching). The relative concentration profiles determined upon etching the whole layer are reported in Fig. 4, for samples obtained from pure iron and cobalt solutions, and in Fig. 5, for samples prepared from mixed solutions with different concentration of Fe^{2+} and Co^{2+} . It can be

seen in Fig. 4(a) that, from a solution containing just Fe^{2+} ions, a considerable part of the electrodeposited single Fe metal accumulates on top surface of the specimen rather than in the PS layer. This is concluded from the obvious decrease in iron atomic concentration from the top surface to the bottom of PS. Conversely, in the case of pure cobalt [Fig. 4(b)], it shows that there is a large concentration of cobalt at the bottom of the nanoporous film. This Co signal covers the entire thickness of the porous layer, but it decreases in intensity from 55 at.% at the bottom to 40 at.% near the top surface of the PS layer. For the current density of $500 \mu\text{A cm}^{-2}$ and the deposition time of 10 min used in the experiment, the deposit also covers the surface of the sample.

Similar profiles as for pure Co are obtained for both iron and cobalt with mixed solutions [Figs. 5(a)–5(c)]. This demonstrates the role played by cobalt in the deposition of iron inside the porous layer and, therefore, in pores filling by Fe–Co deposit. This role seems crucial, since a small amount (5 at.%) of cobalt ion in the solution is enough to cause iron nucleation to start at the pore tips [Fig. 5(a)]. This is indicated by the appearance of an important iron peak (24 at.%) in the bulk of PS, which is not observed in the case of pure iron [Fig. 4(a)]. However, for this low concentration of cobalt, the maximum pore-filling rate (Fe + Co) is small (30 at.% only) in

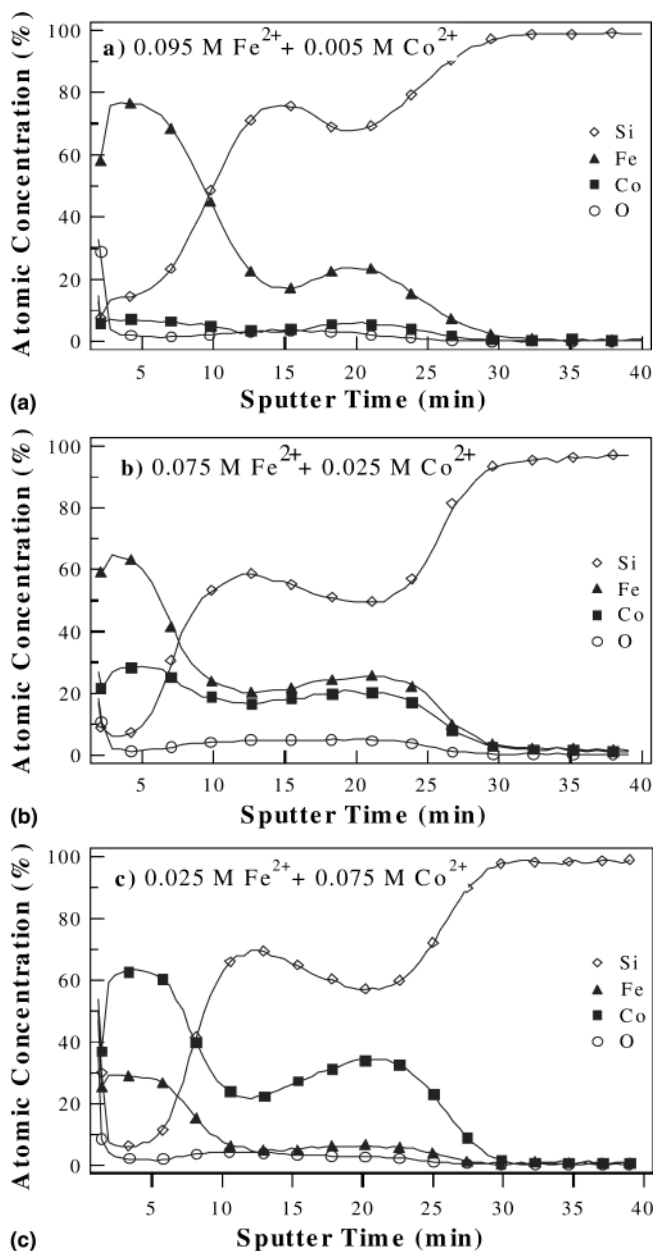


FIG. 5. Auger depth profile concentration of iron, cobalt, silicon, and oxygen performed by ion etching in a $0.3\text{-}\mu\text{m}$ *p*-type porous layer electroplated by Fe–Co alloys.

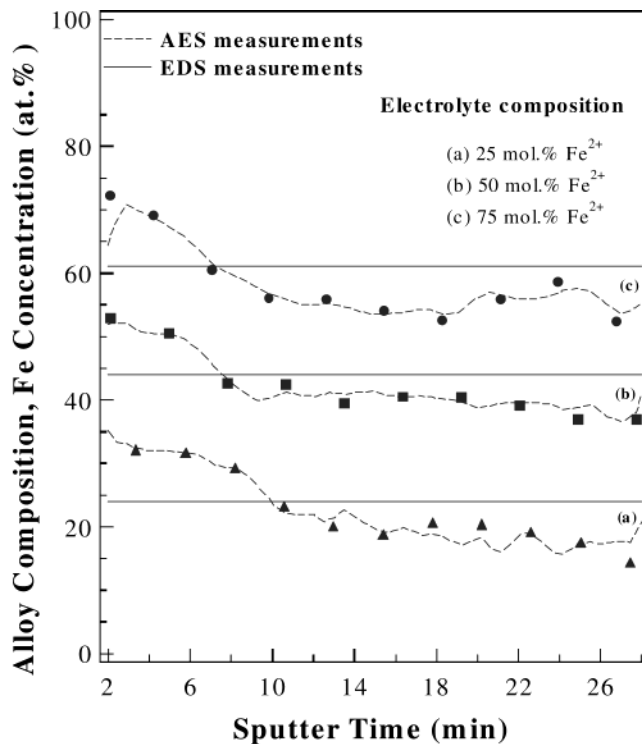


FIG. 6. Plot of the iron concentration (in atomic percent) versus the sputter time, obtained from AES depth profiling for three different concentrations in weight percent in the electrolyte. Horizontal lines correspond to the average iron concentrations measured by EDS analysis.

comparison with that of pure cobalt (55 at.%) that nearly matches up to the porosity of the layer (60%). Besides, it is easy to see that, for all solutions, iron content is reduced with respect to Fe^{2+} concentration in the electroplating bath. In particular, at the maximum pore-filling rate (after 20 min in etching), Fe composition (defined as in EDS measurements with both Fe and Co contents directly determined from AES profiles) is around 80 at.% Fe for 95 mol% Fe^{2+} in Fig. 5(a), 55 at.% Fe for 75 mol% Fe^{2+} in Fig. 5(b), and 15 at.% Fe for 25 mol% Fe^{2+} in Fig. 5(c). It is also easy to see that the growth of iron-poor deposits occurs inside the pores. This feature is clearly presented in the Fig. 6 (dashed line), where the variation of Fe composition in Fe–Co deposit is plotted versus the sputter time, for three different compositions of the electroplating bath. Indeed, Fe–Co deposits grow practically with a constant Fe composition, with two regions being observed: the capping layer and inside the pores. In the capping layer, Fe composition is at least close to that of the electroplating bath. Inside the pores, iron content is lowered with regard to its concentration in the deposition bath.

From the Figs. 4 and 5, it can be also seen that the samples prepared using our procedure contain oxygen that is distributed all along the thickness of the layer. The front surface of the sample is highly oxidized, resulting from its exposure to air after deposition. The oxygen signal is about 1–2 at.% in the capping layer and rises quickly to a nearly flat low concentration level of 3–5 at.% throughout the PS layer thickness. The fact that the oxygen signal is almost absent within the deposit that covers the PS surface indicates that metal hydroxides do not form during iron and/or cobalt electrodeposition. Thus, the partial oxidation observed within the PS layer of the samples is probably located at the pores wall.

E. Fourier transform infrared spectroscopy (FTIR)

EDS techniques characterize only atomic concentration of the elements, and AES was only used for this work in that mode. To check if oxygen is really linked to silicon and which step of the process is involved in the oxidation, the samples were also characterized by Fourier transform infrared spectroscopy (FTIR). FTIR analyses were performed on freshly prepared samples, and the different steps of the sample preparation were examined (Figs. 7–9). For all spectra, the baseline has been manually corrected. For the as-formed PS, the analyses were carried out on samples with a porous layer thickness greater than 1 μm . In the case of the metallized samples, a porous layer thickness of 0.6 μm was chosen to avoid any modification of the electrodeposition process by reaching the p^+/p interface located approximately at a depth of 0.8 μm . For such samples, a porosity of 80% was chosen to increase the internal surface of the layer and then the IR signal arising from the porous layer.

Figure 7 shows FTIR spectra obtained for a PS (60%) layer (approximately 1 μm) formed by anodization at a constant current density of 0.3 mA cm^{-2} for 80 min (spectrum a) and for the same sample subjected to the treatments (before the metal electroplating) described in Sec. II.A [spectra (b) and (c)]. The as-formed nanopore walls are covered with an important concentration of hydrogen termination. Strong absorptions are observed in the ranges 500–700, 880–930, and 2020–2180 cm^{-1} . According to Table I, absorption peaks at 519 and 627 cm^{-1} are attributed to Si activated by F atoms and to the stretching mode of Si–Si bonds, respectively. All other major peaks can be associated with silicon atoms linked to one, two, or three hydrogen atoms: the peak at

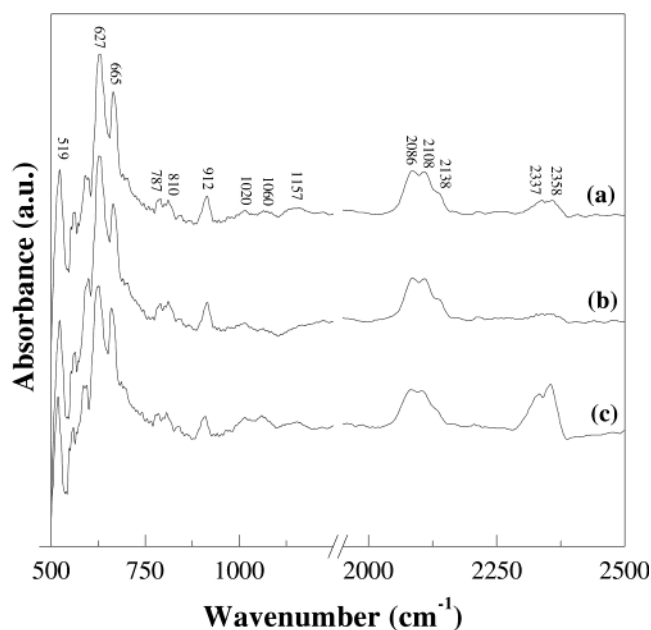


FIG. 7. Typical relative FTIR absorption spectra of porous *p*-type silicon prepared in the dark: (a) as-formed; (b) after dip in ethanol and then in 5% HF and rinsed in $\text{H}_2\text{O/DI}$; (c) after immersion in iron and cobalt sulfates electrolyte for 20 min in the dark.

TABLE I. Description of the IR modes observed in a freshly prepared porous silicon.

Frequency (cm^{-1})	Mode description	Ref.
517–519	TO, Si activated by F	26
625	Si–Si stretching	27–29
665	SiH wagging or bending	26, 29, 30
912	SiH ₂ scissor or bending	26–30
950–1250	Si–O–Si stretch	26–31
2086	SiH stretch	26, 27, 29, 30
2108	SiH ₂ stretch	26, 27, 29, 30
2138	SiH ₃ stretch	26
2337	?	
2358	?	26

665 cm^{-1} is due to the bending mode of the monohydride Si–H, that at 912 cm^{-1} is due to the scissoring mode of the dihydride Si–H₂, and the triplet at 2086, 2108, and 2138 cm^{-1} is from stretching vibration modes of monohydride, dihydride, and trihydride. On the contrary, there is no significant peak between 950 and 1250 cm^{-1} that should indicate the presence of Si–O bonds. In addition, no shoulder to the triplet between 2150 and 2300 cm^{-1} corresponding to a partial oxidation of the hydride species^{30,31} is observed in our samples. Therefore, the internal surface of as-formed PS contains almost no oxygen. This is consistent with AES depth profile data for as-formed PS not shown previously.

Note however the presence in the spectrum of two peaks at 2337 and 2358 cm^{-1} . The peak at higher wave number has already been reported in the literature but not identified.²⁶ These two neighboring peaks are apparently due to the residual electrolyte remaining in the pores after preparation, as suggested by the analysis of all spectra studied here. As a first information about these two peaks, their intensities decrease after the sample dip in 5 at.% HF and a rinse in deionized water (spectrum b). This indicates that the hydrophobic properties of the sample are improved, implying that the as-formed PS must contain, all the same, a small amount of oxygen that is below the AES and FTIR detection limits. The intensities of the same peaks increased after immersion in iron and cobalt sulfates solution for 20 min (spectrum c), which indicates a penetration of the electrolyte in the pores.

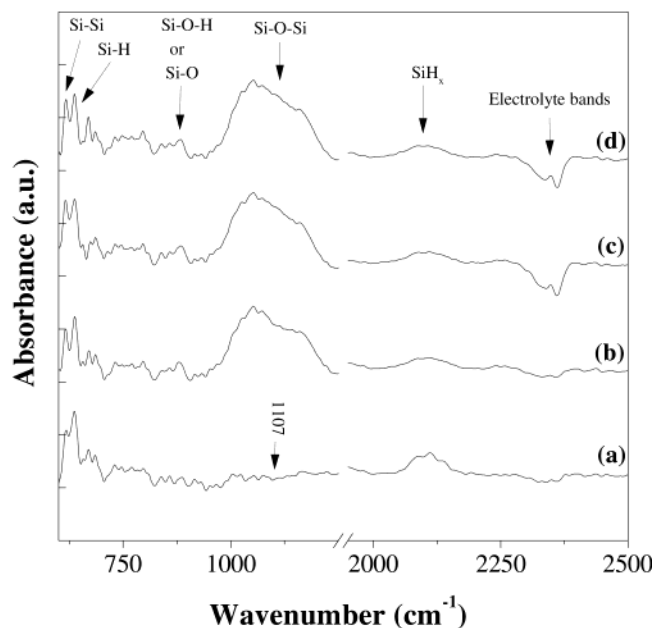


FIG. 8. Typical relative FTIR absorption spectra of impregnated porous *p*-type silicon with Fe–Co electrodeposit: (a) as-formed; PS electroplated at 0.5 $\mu\text{A cm}^{-2}$ for (b) 4 min, (c) 6 min, and (d) 8 min.

After immersion in the electroplating bath, three small peaks (1020, 1060, 1157 cm^{-1}) also appear in the spectrum c (Fig. 7) around the Si–O peak. This weak modification of the absorption observed in the 950–1250- cm^{-1} range means that a slight amount of oxygen, revealed by AES in metallized samples, is introduced at this stage of the sample preparation. More precisely, this stage consists of the immersion of the as-formed PS in the electroplating bath under open-circuit conditions for 20 min prior to the deposition. In return, it is interesting to notice that there is no significant change in the total Si–H content after this preparation step, attesting that silicon passivation with hydrogen termination is not affected.

FTIR spectra of the metallized samples are quite different from that of the as-formed PS as can be seen in the Fig. 8. The most striking feature of the electroplated PS spectra b–d, when compared with the as-formed PS one (spectrum a), is the large increase in intensity of the absorbance in the 950–1250- cm^{-1} range, characteristic of Si–O bonds. In addition, a new band is observed at 880 cm^{-1} that can be assigned to Si–O or Si–O–H. These observations are consistent with the AES results and, moreover, indicate that silicon in the porous layer has been oxidized during the deposition process. This oxidation occurs within the first 4 min of the deposition process since, with increasing deposition time, one may notice that there is no more significant change in the

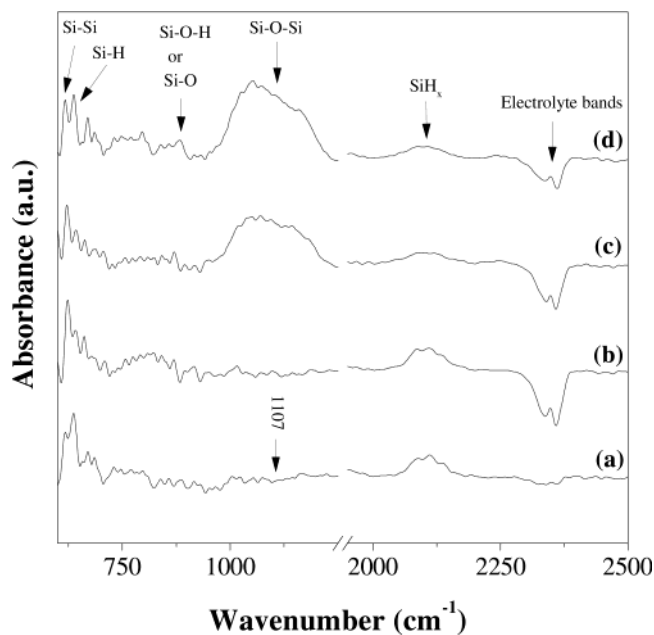


FIG. 9. Typical relative FTIR absorption of the following: (a) as-formed PS; (b) PS cathodically polarized at 0.5 $\mu\text{A cm}^{-2}$ for 8 min in 0.4 M H_3BO_3 electrolyte; (c) in 0.4 M H_3BO_3 + 0.1 M FeSO_4 electrolyte; (d) in 0.4 M H_3BO_3 + 0.025 M FeSO_4 + 0.075 M CoSO_4 electrolyte.

Si–O spectral regions. It can also be seen that a part of the triplet SiH_x hydrides has been lost during the metalization. But it is difficult to determine from the FTIR spectra whether the broken Si–H bonds during the electroplating are directly replaced by Si–O, Si–O–H, or metal–Si ones. Therefore, the chemical mechanism leading to oxidation of silicon in PS during Fe–Co deposition is still unclear.

However, the study of the influence of the electrolyte composition on the FTIR response of the samples (see Fig. 9) allows us to conclude that the oxidation of samples is directly related to the presence of Fe²⁺ and Co²⁺ species in the solution. Indeed, when PS is exposed to an electrolyte containing only boric and sulfuric acids (spectrum b), and the same current density (500 μA/cm² for 8 min) as that used for the deposition is applied, FTIR analysis reveals that only the intensity of the so-defined electrolyte peak situated around 2300 cm⁻¹ is considerably increased. In particular, there is no change in the absorption of Si–O bonds with regard to as-formed PS (spectrum a). This implies that, in the absence of both Fe²⁺ and Co²⁺ ion in the solution, porous silicon is cathodically protected from the ambient. On the contrary, as already mentioned above (Fig. 8), PS is oxidized in mixed Fe–Co sulfate solutions (spectra d in Fig. 9). Curiously, the absorbance in the 950–1250-cm⁻¹ range appears less important after pure iron deposition (spectrum c).

IV. DISCUSSION

The electrodeposition of Fe and Co metals into porous silicon was performed in the galvanostatic mode. Their individual formation proceeds from charge transfer at the substrate, according to the following reduction reaction:



which is always accompanied by hydrogen bubbles evolution:



Prior to the deposition in galvanostatic mode, the electrochemical behavior (current–potential characteristic) of the substrate/electrolyte interface is studied for different concentrations of the electroactive Fe²⁺ and Co²⁺ species. We have observed that pure Co and pure Fe deposited onto PS/Si substrate at practically the same cathodic overpotential that is around –0.85 V/Ag–AgCl. An appreciable variation between the reduction potentials of these two metals was observed when they were deposited directly on nonporous silicon. On polished silicon, cobalt deposits first according to its redox potential, which is

more cathodic than that of iron. These two observations will help the understanding of the fact that cobalt deposits preferentially to iron inside the pores. This aspect of the work will be discussed in details in a forthcoming paper. When there are both Fe²⁺ and Co²⁺ species in the solution, we have seen that the nucleation on porous substrate occurred at a unique overpotential, which is also closer to that of pure iron and cobalt deposition. Such a unique onset potential could be attributed to the deposition of single Fe metal. In that case, iron would inhibit the codeposition of Co, the more noble metal, according to the anomalous codeposition of iron-group alloys.^{18,32} However, the observation of the nucleation at only one cathodic potential is more likely associated with the codeposition of Fe and Co metals through the reduction of Fe²⁺ to Fe and Co²⁺ to Co, as demonstrated from our detailed analysis of the sample compositions by EDS and AES techniques. Therefore, the deposition of Fe and Co at the same potential (–0.85 V/Ag–AgCl) appears as a characteristic of the electrodeposition of Fe–Co alloys. In addition, the deposition potential of Fe–Co alloys does not vary with the bath composition. This might be due to the fact that, in our experiments, both the molarity and the pH of the electrolyte were maintained constant. However, additional information by x-ray diffraction analysis of the samples is necessary to check the structure of the deposits.

As revealed by EDS measurements, iron-poor deposits with respect to the bath composition were formed (compare solid and horizontal lines to Fe²⁺ concentrations in Fig. 6). This feature is quite astonishing for Fe–Co alloys. As mentioned above, it is well known that the electrodeposition behavior of binary iron-group alloys belongs to Brenner's anomalous codeposition category, in which the less noble metal (iron in our case) deposits preferentially to the more noble metal.³² This behavior is due to an inhibition effect of the less noble metal on the codepositing more noble metal. It has been stated in the literature that inhibition is due to partial surface blocking by an intermediate adsorbed reaction of the less noble species (Fe²⁺ in our case). This phenomenon is usually accompanied by the formation of hydroxide ions, MeOH⁺, which play an important role in anomalous codeposition.³³ Apparently, this so-called anomalous Co deposition of binary iron-group alloys seems not completely appropriate to the case of Fe–Co systems, as it has been reported in some earlier studies^{19,20} These studies have demonstrated that it is possible to deposit Fe–Co alloys with the same Co:Fe ratio of the solution. However, our results do agree neither with the conclusion of Refs. 19 and 20 nor with the anomalous codeposition phenomenon of iron-group systems.

AES measurements allowed us to understand this apparent discrepancy between our results and those reported in the literature. The major specificity of our

experiments lies in the fact that the substrate consists of a porous and semiconductor material. The deposition of iron-poor Fe–Co alloys is probably due to the fact that, inside the pores, the deposition of cobalt is promoted and that of iron is practically prevented (Fig. 4). This result is rather expected from semiconductor electrochemistry than from the chemical standpoint (inhibition effect). Indeed, it has been previously shown, from the AES in-depth profile concentration, that the deposition of pure iron is concentrated near the PS top surface [Fig. 4(a)]. Therefore, its nucleation might take place all over the pore walls. Assuming this, most of the current flow from the solution into the substrate could occur through the silicon nanocrystallites. This suggests that porous silicon skeleton impregnated with the pure iron-based electrolyte is always conductive.

Contrary to pure iron, the pores are filled with pure Co. The behavior of the distribution of the Co atoms observed in this work [Fig. 4(b)] was to our knowledge never reported before in the case of electrodeposited metals into porous silicon. It is different from that obtained for iron into porous *n*-type silicon⁴ and other metals,^{6,7,9} where the amount of metal, instead of a decrease, has increased from the bottom to the top of the pores. The existence of an important amount of the deposit at the pore bottom has been, nevertheless, reported by Steiner for indium deposited into porous *n*-type silicon.⁸ It has been attributed to the fact that the nucleation started at the pore bottom, assuming that, by analogy to porous silicon formation, most of the nanoparticles are electrically insulated from the bulk silicon. However, the decrease of cobalt concentration from the bottom to the top surface of PS indicates that the porous skeleton impregnated with Co-based solutions becomes conductive beyond a certain time of deposition.

Different models have been proposed to understand the electrical transport properties of porous silicon.^{34–39} In many works, it is assumed that the carriers are transported by diffusion from the substrate to the PS. According to the conclusion of Bsiesy and co-workers,³⁷ the free charge carriers can flow through the porous skeleton if their flux is not the limiting factor in the current conduction process. In the case of porous silicon impregnated with an electrolyte, this is possible when the diffusion of ions in the electrolyte, or the charge exchange rate at the substrate/electrolyte interface, is the limiting factor.³⁷ Assuming this, the behavior of the distribution of cobalt in porous silicon can be interpreted as follows. At the beginning of the deposition, the current should be rather limited by the free charge carrier supplied by silicon at the bottom of the porous silicon. The charge exchange should then be principally concentrated at the pores bottom, and then Co should nucleate there. However, as and when the deposition proceeds, the reduction of Co^{2+} to Co should lead to the decrease of the electrolyte

concentration inside the pores. Such a depletion of the electroactive species concentrations inside the pores should not only slow down the deposition process, but it could cause it to occur preferentially on the top surface of the porous layer. Indeed, when the concentration of the electrolyte is lower inside than outside the pores, the ion diffusion in the electrolyte becomes the limiting factor of the current. The thickness of the porous layer (0.3 μm) being quite lower than that of the diffusion layer, ions diffusing from the electrolyte are consumed by the electrochemical reactions over a thin layer located on the top of the porous structure.

To support our interpretation, we have performed an experiment where the deposition of iron–cobalt is stopped after 2.5, 5, and 7.5 min and the electrolyte in the electrochemical cell was renewed after each stop. Iron and cobalt concentration profiles corresponding to such conditions are presented in Fig. 10. It can be seen in comparison with the data from Fig. 5(c) that the electrolyte renewal changes the behavior of both Fe and Co distributions but only inside the pores. Indeed, the composition of the capping layer remains uniform and unchanged (32 at.% Fe). The main difference is that a more homogeneous filling of the pores is achieved. This implies that electrolyte renewal ensures the recovery of the solution concentration inside the pores. Another obvious feature of Fig. 10 is that iron content is increased inside the pores, from 19 at.% Fe in Fig. 5(c) to 28 at.% Fe (greater than Fe^{2+} concentration in the bath) in Fig. 10. This confirms that iron deposition is more likely controlled by mass transport than that of cobalt.

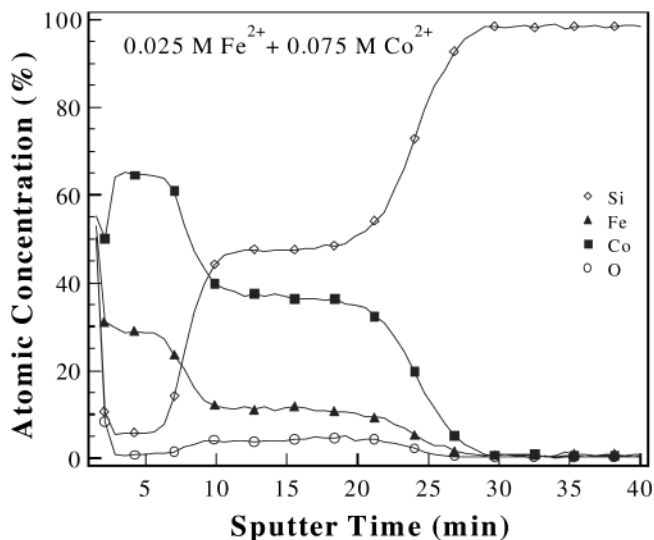


FIG. 10. Auger depth profiles of iron, cobalt, silicon, and oxygen performed by ion etching in a 0.3- μm *p*-type porous layer electroplated by Fe–Co alloys with intermittent electrolyte renewal.

On the whole, our results indicate that the transport mechanisms in porous *p*-type silicon are completely different depending on the kind of electrolyte used to fill the pores: pure iron-based electrolyte or cobalt-based solutions. This probably comes to the fact that the cathodic standard potentials of these two metals are different and might be discussed in light of a detailed description of the charge transport within PS band structure at PS/electrolyte and Si/electrolyte interfaces. This requires further investigations on the band structure of porous silicon formed from a *p*-type silicon substrate.

Some applications of metallized porous silicon network, such as the synthesis of metal silicides, require oxide-free systems. From the AES sputter depth profile it has also been noticed that oxygen was present in our samples up to a concentration of 5 at.%. FTIR analyses allowed us to see that a considerable part of oxygen content was localized at the pore walls, introduced during the deposition process and intimately related to the presence of Fe²⁺ and Co²⁺ species in the solution. The presence of silicon oxide between the electrodeposit and the pore walls was not expected, since as-formed PS was found by FTIR and AES analyses to be practically oxide-free and is normally electrically protected even during cathodic metal deposition. It has been moreover established, in the literature, that a binary Si/metal system can be built without oxidation of PS.^{6,40} In our samples, the oxidation process of silicon may be associated either with the confinement by the deposit of oxygen present in the electrolyte that was not deaerated or possibly with electroless deposition which occurred certainly at the beginning of the deposition.^{4,6,41}

V. SUMMARY AND CONCLUSION

This work demonstrates that it is possible to achieve homogeneous filling of porous *p*-type silicon with electrodeposited pure Co metal and Fe–Co alloys. The determination by EDS of the average alloy composition versus the related bath composition shows an unexpected deficit in iron. This deficit instead of an excess in less noble metal is explained by the fact that Co deposition is electrically promoted into the pores as revealed by the AES measurements. Auger study shows that pure Co deposition starts at the pore bottom, while the nucleation of pure Fe occurs all over the pore walls leading to a preferential deposition on the top surface of the porous layer. In the mixed solutions, the reaction rate of iron inside the pore is catalyzed by cobalt and accounts for a filling of the pores with Fe–Co alloys. Indeed, a small amount (5 at.%) of cobalt in the solution is enough to cause iron nucleation to start at the pore tips.

Furthermore, it is deduced from both AES and FTIR studies that almost no trace of oxygen is found in the as-formed PS and the pore walls are covered with

hydride species. On the other hand, the metal deposition process oxidizes the structure, and the oxygen detected by AES in metallized PS is localized mainly at the pore walls as seen by FTIR measurements. The present experimental results suggest that, in contact with pure Co electrolyte, the porous skeleton is electrically isolated from the bulk silicon, at least at the beginning of the deposition process. On the contrary, PS is always conductive when contacted by pure Fe electrolyte. Hence our study provides further experimental data to analyze the mechanism responsible for the incorporation of metals into the pores. A complete understanding of the deposition process requires, however, further knowledge about the transport mechanisms in the porous silicon and the band bending at Si/electrolyte and PS/electrolyte interfaces. These new results involving the deposition of iron-group materials into cylindrical nanoporous *p*-type silicon might be useful for future silicon technologies.

ACKNOWLEDGMENTS

This work performed at the PCPM laboratory was supported in part by the Secretariat à la Coopération Internationale, Université Catholique de Louvain. Additional experiments involving FTIR measurements were performed at the LPC Laboratory, Institut des Matériaux de Nantes. The authors gratefully acknowledge the supply of implanted silicon wafers by V. Bayot, C. Renaux, and B. Katschmarskyj. We thank R. Morlat and E. Ferain for assistance with SEM and EDS analyses. We are obliged to J-L. Delplancke, for useful discussions about the electrochemical aspect of this work, and to Y. Baltog, for fruitful discussions about porous silicon and FTIR characterizations. F.H. also gratefully acknowledges encouragements from J-P. Michenaud.

REFERENCES

1. R. Hérino, *Mater. Sci. Eng.*, B **69–70**, 70 (2000).
2. C. Renaux, V. Scheuren, and D. Flandre, *Micrelectron. Reliab.* **40**, 877 (2000).
3. X.J. Li, De L. Zhu, Q.W. Chen, and Y.H. Zhang, *Appl. Phys. Lett.* **74**, 389 (1999).
4. F. Ronkel, J.W. Schultze, and R. Arens-Fischer, *Thin Solid Films* **276**, 40 (1996).
5. B.J. Aylett, I.S. Harding, L.G. Earwaker, K. Forcey, and T. Giaddui, *Thin Solid Films* **276**, 253 (1996).
6. M. Jeske, J.W. Schultze, M. Thönissen, and H. Münder, *Thin Solid Films* **255**, 63 (1995).
7. T. Ito, T. Yoneda, K. Furuta, A. Hatta, and A. Hiraki, *Jpn. J. Appl. Phys.* **34**, L649 (1995).
8. P. Steiner, F. Kozłowski, and W. Lang, *Thin Solid Films* **255**, 49 (1995).
9. S.O. Izidinov, V.N. Nazarov, and O.E. Shcheglov, *Russ. J. Appl. Chem.* **68** (Part 1), 519 (1995).
10. S.A. Gusev, N.A. Korotkova, D.B. Rozenstein, and A.A. Fraerman, *J. Appl. Phys.* **76**, 6671 (1994).

11. D.G. Anderson, N. Anwar, B.J. Aylett, L.G. Earwaker, M.I. Nasir, J.P.G. Farr, K. Stiebahl, and J.M. Keen, *J. Organomet. Chem.* **437**, C7 (1992).
12. T. Ito, A. Yamama, A. Hiraki, and M. Satou, *Appl. Surf. Sci.* **41/42**, 301 (1989).
13. S.S. Tsao, R.S. Blewer, and J.Y. Tsao, *Appl. Phys. Lett.* **49**, 403 (1986).
14. R. Herino, P. Jan, and G. Bomchil, *J. Electrochem. Soc.* **132**, 2513 (1985).
15. N. Tsuya, Y. Saito, H. Nakamura, S. Hayano, A. Furugohri, K. Ohta, Y. Wakui, and T. Tokushima, *J. Magn. Magn. Mater.* **54–57**, 1681 (1986).
16. T.M. Whitney, J.S. Jiang, P. Searson, and C. Chien, *Science* **261**, 1316 (1993).
17. L. Piraux, J.M. George, J.F. Despres, C. Leroy, E. Ferain, R. Legras, K. Ounadjla, and A. Fert, *Appl. Phys. Lett.* **65**, 2484 (1994).
18. N. Zech, E.J. Podlaha, and D. Landolt, *J. Appl. Electrochem.* **28**, 1251 (1998).
19. J. Ebothé and S. Vilain, *J. Phys. D: Appl. Phys.* **32**, 2342 (1999).
20. E.M. Kakuno, D.H. Mosca, I. Mazzaro, N. Mattoso, W.H. Schreiner, and M.A.B. Gomes, *J. Electrochem. Soc.* **144**, 3222 (1997).
21. E.M. Kakuno, R.C. da Silva, N. Mattoso, W.H. Schreiner, D.H. Mosca, and S.R. Teixeira, *J. Phys. D: Appl. Phys.* **32**, 1209 (1999).
22. W. Bohne, G.U. Reinsperger, J. Röhrich, G. Röscher, and B. Selle, *Nucl. Instrum. Methods Phys. Res. Sect. B* **136–138**, 273 (1998).
23. S. Hong, C. Pirri, P. Wetzel, and G. Gewinner, *Phys. Rev. B* **55**, 13040 (1997).
24. S. Teichert, R. Kilper, T. Franke, J. Erben, P. Häussler, W. Henrion, H. Lange, and D. Panknin, *Appl. Surf. Sci.* **91**, 56 (1995).
25. *MultiPak Software Manual V5.0*, Part No. 638366, Rev. A, 02 Oct. 1997 (Physical Electronics, Inc., Eden Prairie, MN, 1994–1997). p. C1.
26. Z.C. Feng, A.T.S. Wee, and K.L. Tan, *J. Phys. D: Appl. Phys.* **27**, 1968 (1994).
27. H. Mizuno, H. Koyama, and N. Koshida, *Appl. Phys. Lett.* **69**, 3779 (1996).
28. J. Hilliard, D. Andsager, L. Abu Hassan, H.M. Nayfeh, and M.H. Nayfeh, *J. Appl. Phys.* **76**, 2423 (1994).
29. T. Ban, T. Koizumi, S. Haba, N. Koshida, and Y. Suda, *Jpn. J. Appl. Phys.* **33**, 5603 (1994).
30. Y.H. Xi, W.L. Wilson, F.M. Ross, J.A. Mucha, E.A. Fitzgerald, J.M. Macaulay, and T.D. Harris, *J. Appl. Phys.* **71**, 2403 (1992).
31. M.A. Hory, R. Hérino, M. Ligeon, F. Muller, F. Gaspard, I. Mihalcescu, and J.C. Vial, *Thin Solid Films* **255**, 200 (1995).
32. A. Brenner, *Electrodeposition of alloys* (Academic, New York, 1963).
33. L.J. Gao, G.W. Anderson, and P.R. Norton, *J. Appl. Phys.* **79**, 5795 (1995).
34. M. Ben-Chorin, F. Möller, and F. Koch, *Phys. Rev. B* **49**, 2981 (1994).
35. N.J. Pulsford, G.L.J.A. Rikken, Y.A.R.R. Kessener, E.J. Lous, and A.H.J. Venhuizen, *J. Appl. Phys.* **75**, 636 (1994).
36. D. Steivenard and D. Deresmes, *Appl. Phys. Lett.* **67**, 1570 (1995).
37. A. Bsiesy, B. Gelloz, F. Gaspard, and F. Muller, *J. Appl. Phys.* **276**, 175 (1996).
38. A.K. Ray, M.F. Mabrook, A.V. Nabok, and S. Brown, *J. Appl. Phys.* **84**, 3232 (1998).
39. D.N. Goryachev, G. Polisskii, and O.M. Sreseli, *Fiz. Tekh. Poluprovodn. (S. Peterburg)* **34**, 221 (2000) [*Semiconductors* **34**, 227 (2000)].
40. M. Jeske, J.W. Schultze, and H. Münder, *Electrochim. Acta* **40**, 1435 (1995).
41. L. Montès, F. Muller, F. Gaspard, and R. Hérino, *Thin Solid Films* **29**, 35 (1997).